Available online at www.sciencedirect.com
ScienceDirect
Journal of Membrane Science 295 (2007) 11–20
journal of MEMBRANE SCIENCE
www.elsevier.com/locate/memsci

Biofouling of reverse osmosis membranes: Role of biofilm-enhanced osmotic pressure

Moshe Herzberg, Menachem Elimelech *

Department of Chemical Engineering, Environmental Engineering Program, Yale University, New Haven, CT 06520-8286, USA

Received 11 November 2006; received in revised form 11 February 2007; accepted 13 February 2007
Available online 20 February 2007

Abstract

A bench-scale investigation of RO biofouling with *Pseudomonas aeruginosa* PA01 was conducted in order to elucidate the mechanisms governing the decline in RO membrane performance caused by cell deposition and biofilm growth. A sharp decline in permeate water flux and a concomitant increase in salt passage were observed following the inoculation of the RO test unit with a late exponential culture of *P. aeruginosa* PA01 under enhanced biofouling conditions. The decrease in permeate flux and salt rejection is attributed to the growth of a biofilm comprised of bacterial cells and their self-produced extracellular polymeric substances (EPS). Biofilm growth dynamics on the RO membrane surface are observed using confocal microscopy, where active cells, dead cells, and EPS are monitored. We propose that the biofilm deteriorates membrane performance by increasing both the trans-membrane osmotic pressure and hydraulic resistance. By comparing the decrease in permeate flux and salt rejection upon fouling with dead cells of *P. aeruginosa* PA01 and upon biofilm growth on the membrane surface, we can distinguish between these two fouling mechanisms. Bacterial cells on the membrane hinder the back diffusion of salt, which results in elevated osmotic pressure on the membrane surface, and therefore a decrease in permeate flux and salt rejection. On the other hand, EPS contributes to the decline in membrane water flux by increasing the hydraulic resistance to permeate flow. Scanning electron microscope (SEM) images of dead cells and biofilm further support these proposed mechanisms. Biofilm imaging reveals an opaque EPS matrix surrounding *P. aeruginosa* PA01 cells that could provide hydraulic resistance to permeate flux. In contrast, SEM images taken after fouling runs with dead cells reveal a porous cake layer comprised of EPS-free individual cells that is likely to provide negligible resistance to permeate flow compared to the RO membrane resistance. We conclude that "biofilm-enhanced osmotic pressure" plays a dominant role in RO biofouling.

Keywords: Biofouling; EPS; *P. aeruginosa*; Biofilm; Fouling; Biofilm-enhanced osmotic pressure; Cake-enhanced osmotic

1. Introduction

The decrease in performance of reverse osmosis (RO) membranes in water reuse and purification systems due to fouling is a major concern [1–5]. Fouling requires frequent chemical cleaning and ultimately shortens membrane life, thus imposing a large economic burden on RO membrane plant operation. The major types of fouling in RO membranes are inorganic salt precipitation (contributed by sparingly soluble salts), organic (mostly natural organic matter or effluent organic matter), colloidal (caused by accumulation of a colloidal cake layer on the membrane surface), and microbiological (usually governed by bacterial biofilm formation).

In natural and engineered aquatic systems, bacteria are often found as biofilms—structured communities of bacterial cells enclosed in self-produced extracellular polymeric substances (EPS), irreversibly associated with solid surfaces [6,7]. Bacteria in RO systems for water and wastewater reuse are no exception. The combination of the inevitable presence of microorganisms in a non-sterile system, the relative abundance of nutrients, and the convective permeate flow through the membrane, will eventually lead to biofilm growth on the RO membrane surface [8,9].

The transport and attachment of suspended bacterial cells to a solid–liquid interface is the first step in biofilm formation. The approach and attachment of bacteria to a surface are mediated by physical, chemical, and biological factors. As bacteria approach the surface, surface–bacteria interactions (such as electrostatic and hydrophobic interactions) start to play an important role [8,10–13], with attachment being generally more favorable with hydrophobic, non-polar surfaces [6]. The hydrophobicity

* Corresponding author. Tel.: +1 203 432 2789; fax: +1 203 432 2881.
E-mail address: menachem.elimelech@yale.edu (M. Elimelech).

0376-7388/$ – see front matter © 2007 Elsevier B.V. All rights reserved.
doi:10.1016/j.memsci.2007.02.024

of the cells also contributes to increased attachment, and may be attributed to fimbriae appendages [14]. "Conditioning" of the substratum with adsorbed macromolecules, originating either from the surrounding solution or from the cells, is suggested to enhance attachment of cells to the surface [15–17]. In addition, flagellar motility is suggested to be necessary for initial attachment, probably to overcome repulsive forces [18,19]. Other factors such as surface roughness, hydrodynamics, and aqueous solution characteristics (pH, nutrient level, ionic strength, and the presence of multivalent cations) are also important factors in initial biofilm formation.

Bacterial cell surfaces contain lipopolysaccharides (LPS) and extracellular polymeric substances, which play a role in bacterial-surface interactions. The O-antigen component of the LPS in *E. coli* has been suggested to shield electrostatic repulsion of charged functional groups or to increase the outer membrane surface roughness [12]. *P. aeruginosa* LPS comprises two types of LPS, which can be characterized by two distinct O-polysaccharides: a high molecular weight B-band and a shorter A-band [20,21]. The surface charge and hydrophobicity of the bacteria are affected by mutations in A- and B-band encoding regions, and these mutations were shown to affect attachment to both hydrophobic and hydrophilic surfaces [22]. EPS also plays an important role at the initial stages of biofilm formation. Synthesis of alginate, one of the major components of *P. aeruginosa* EPS, was shown to be up-regulated upon contact of the cells with a surface [23]. The relationship between alginate expression, cell motility, and biofilm formation has been studied by Wozniak and co-worker [24].

Further biofilm growth takes place by auto-aggregation and microcolony formation of the attached cells. In *P. aeruginosa*, this process is mediated by surface translocation through twitching motility, attributed to type IV pili [25]. Following attachment, EPS synthesis is increased. The EPS in *P. aeruginosa* biofilms contains alginate and other polysaccharide components, some of which have yet to be identified [26–29]. Other components of EPS include proteins, lipids, and DNA [30,31].

Fundamental studies on biofouling of RO or nanofiltration (NF) membranes are rather scarce. Flemming et al. [9,31,32] described biofilm development on RO membranes and the consequences of biofouling, most notably flux decline and decrease in salt rejection. Biofouling case studies of NF and RO membranes were used to establish protocols for diagnosis, prediction, and prevention of biofouling [33]. Physical, physiological, and chemical analyses were used to characterize biofouling of RO membranes by *Mycobacterium* sp., *Acinetobacter*, and *Flavobacterium-Moraxella* [34,35]. Recently, Ivnitsky et al. [36] characterized the effect of biofilm growth on NF membrane performance in a wastewater treatment process by using both synthetic and real wastewater. That study also provided a characterization of the bacterial species in the biofilm, as well as FTIR analysis of the biofouling layer, which indicated that proteins and amino acids had accumulated on the membrane. A recent study by Schnieder et al. [8] suggested that reducing biofouling in RO systems is largely dependent upon reducing the assimilable organic carbon together with a continuous biocide addition. While the above studies provided useful qualitative information on biofouling of RO and NF membranes, none of these studies elucidated the mechanisms by which biofouling influences permeate flux and salt rejection behavior.

Biofouling of RO membranes is always followed by a decrease in permeate water flux, and, in most cases, a decrease in salt rejection is also observed [4,8,34–38]. Fouling mechanisms of RO membranes by colloidal particles, dissolved organic matter, and salt precipitation (scaling) have been systematically studied and elucidated. Flux decline in organic matter or precipitate fouling of RO membranes is attributed to the increase in hydraulic resistance by the fouling layer [39–41]. In colloidal/particulate fouling of RO membranes, the decrease in permeate water flux is mostly attributed to cake-enhanced osmotic pressure [42,43]. However, to date, the mechanisms for the decrease in RO membrane performance upon biofilm formation have not been elucidated.

The objective of this paper is to elucidate the mechanisms of RO membrane biofouling and the consequent effects on permeate flux and salt rejection. Well-controlled, short-term accelerated biofouling experiments with a model bacterium, *P. aeruginosa* PA01, were conducted using a laboratory-scale RO test unit. The mechanisms by which the bacterial cells and their self-produced EPS influence permeate flux and salt rejection were investigated by conducting fouling experiments with dead cells (i.e., no EPS produced), by imaging the different fouling layers with a scanning electron microscope (SEM), by imaging the dynamics of biofilm growth with a laser scanning confocal microscope (LSCM), and by measuring the effects of biofilm formation on membrane performance. Short term, accelerated biofouling experiments with a mono-culture biofilm or with dead cells, like those presented in this paper, allow the elucidation of the fundamental mechanisms involved in biofouling of RO membranes.

2. Materials and methods

2.1. Model bacterial strain and media

A derivative of *P. aeruginosa* PA01 chromosomally encoding short-life GFP, PA01 AH298, was kindly received from S. Molin [44], the Technical University of Denmark. This strain is tellurite resistant (150 μg/mL) and its GFP expression is growth dependent due to the $rrnBp_1$ promoter located upstream of the *gfp* gene. A fresh single colony of PA01 AH298 (pre-grown on LB [45] agar supplemented with tellurite) was used as inoculum for an overnight culture grown in LB broth. This overnight culture was re-diluted in LB broth and grew to late exponential phase with a final optical density (600 nm) of 1, to be used as inoculum for the biofouling experiments.

An enriched synthetic wastewater medium was used for bacterial growth in the RO crossflow test unit. The chemical composition chosen for the synthetic wastewater was based on secondary effluent quality from selected treatment plants in California with high rate biological processes [46]. In order to achieve an enhanced biofouling behavior, a relatively high carbon and high energy source, together with 1:1000 dilution of

LB broth, were supplemented to the wastewater media. Specifically, to prepare the synthetic wastewater, deionized (DI) water (Nano Pure II, Barnstead, Dubuque, IA) was supplemented as follows: 1.16 mM sodium citrate, 0.94 mM ammonium chloride, 0.45 mM KH_2PO_4, 0.5 mM $CaCl_2{\cdot}2H_2O$, 0.5 mM $NaHCO_3$, 2.0 mM NaCl, and 0.6 mM $MgSO_4{\cdot}7H_2O$. In addition, 1 mL of LB broth was added per 1 L of DI water. The final pH was 7.4 and the calculated ionic strength was 14.6 mM. All chemicals were ACS grade (Fisher Scientific, Pittsburgh, PA).

2.2. RO membrane and crossflow test unit

A commercial thin film composite reverse osmosis membrane, LFC-1 (Hydranautics, Oceanside, CA), was used as a model membrane for the biofouling experiments. The hydraulic resistance was determined to be 1.06 ($\pm$0.018) $\times 10^{14}$ m^{-1} at 25 °C. The observed salt passage was 2.11 $\pm$ 0.44%, as determined using the synthetic wastewater described above at an applied pressure of 12.42×10^5 Pa (180 psi or 12.42 bar) and a crossflow velocity of 8.5 cm/s. The membrane was received as a flat sheet and stored in DI water at 4 °C. Physical and chemical properties of the LFC-1 membrane can be found in our previous publication [47].

A laboratory scale test unit, similar to that described in our previous publications [48,49], was used for the biofouling experiments. The unit comprised a membrane crossflow cell, high-pressure pump (Hydra-Cell, Wanner Engineering Inc.), feed water reservoir, chiller equipped with a temperature control system (Neslab RTE-7, Thermo Electron), and a data acquisition system (PC interfaced), used to acquire the permeate flow rate (Optiflow 1000 flowmeter, Humonics, CA), conductivity (Accumet AR60, Fisher Scientific), and dissolved oxygen concentration (Accumet AR60, Fisher Scientific). Retentate flow rate was monitored with a floating disk rotameter (King Instrument, Fresno, CA). The dimensions of the rectangular, crossflow, channel membrane unit were 7.7 cm $\times$ 2.6 cm with a channel height of 0.3 cm. Both permeate and retentate were recirculated back to the feed reservoir, limiting the well controlled biofouling experiments to short time periods of batch growth conditions.

2.3. Biofouling protocol

A biofouling protocol was developed that allows accelerated bacterial deposition and growth on the membrane surface. A thorough cleaning of the unit at the beginning and the end of every experiment was conducted. Before every experiment and prior to inserting the RO membrane coupon, the RO unit was disinfected and thoroughly cleaned to remove trace organic impurities by applying the following steps: (1) recirculation of 0.5% sodium hypochlorite for 2 h, (2) rinsing the unit twice by recirculating tap water for 10 min, (3) cleaning trace organic matter by recirculation of 5 mM EDTA at pH 11 for 30 min, (4) repeating step 2, (5) additional cleaning of trace organic matter by recirculation of 2 mM SDS at pH 11 for 30 min, (6) repeating step 2, (7) sterilizing the unit by recirculation of 95% ethanol for 1 h, (8) rinsing the unit three times with DI water (heterotrophic count of the DI water was less than 10 bacterial cells per mL) to eliminate ethanol residues, and (9) inserting the LFC-1 membrane coupon.

Following this sterilization/cleaning protocol, the membrane was compacted with DI water at a pressure of 20.68×10^5 Pa (300 psi or 20.68 bar) until the permeate flux attained a constant value (usually after 12–18 h). Following compaction of the membrane, a 1 h baseline performance with DI water at 12.42×10^5 Pa (180 psi (12.42 bar)) and 25 °C was conducted, with this pressure and temperature being maintained during all of the experiments. After attaining stable flux with DI water, the previously described synthetic wastewater was added to the feed reservoir, except for the 1 mL LB broth per liter of media and the 0.94 mM ammonium chloride. With this electrolyte solution, the system was equilibrated for 5 h. After this stage, a culture of PA01 AH298 was washed three times with an electrolyte solution identical to the one used in the fouling experiments. Ten milliliters of PA01 AH298 (late exponential growth phase) with a final optical density (600 nm) of 1 were centrifuged for 10 min at 8000 rpm and 4 °C, and re-suspended by vortexing. The washed PA01 AH298 exponential phase culture was inoculated into the feed reservoir to achieve an initial cell concentration of 10^7 cells/mL. The bacteria were recirculated within the unit, allowing cell deposition to occur on the RO membrane for 30 min, followed by the addition of LB and ammonium chloride. Samples from the permeate and the feed reservoir were collected at all stages for determination of TOC and conductivity. Oxygen concentration in the feed reservoir during the experiments varied between 3.2 and 3.5 mg/L. For the control experiment without bacteria, all nutrients, including diluted LB broth (1/1000) and ammonium chloride, were added after a 1 h baseline performance run with DI water.

Fouling experiments with dead cells of PA01 AH298 were conducted in the same way, with an initial cell concentration of 10^9 cells per mL. As will be discussed later, the objective of the experiments with dead cells was to better understand the membrane biofouling mechanism. Dead cells of PA01 AH298 were prepared from 1 L of late exponential culture, grown in LB broth (optical density of 1 at 600 nm), washed twice with 150 mM NaCl, (centrifuged for 10 min at 8000 rpm and 4 °C and resuspended by vortexing), and incubated in 400 mL of 4% buffered formaldehyde solution for 2 h at room temperature. The formaldehyde solution was supplemented with 4 g/L NaH_2PO_4 and 6.5 g/L Na_2HPO_4 reaching a pH of 6.6. After fixation of the bacteria, the cells were washed three times with an electrolyte solution identical to that used in the fouling experiment, centrifuged for 10 min at 8000 rpm and 4 °C, and resuspended by vortexing. The formaldehyde-fixed cells were added 5 h after the unit had been equilibrated with the electrolyte solution. Two millimolars of sodium azide (instead of 2 mM NaCl) were added to prevent any possible growth in the synthetic wastewater. No sodium azide was added to the other set of fouling experiments with dead cells in DI water, which were supplemented with 0.01 mM lanthanum chloride ($LaCl_3$). The absence of sodium azide in these experiments was necessary to keep the ionic strength very low as is described later in the paper.

2.4. Analytical methods

For determination of salt rejection, conductivities of both the feed and permeate were measured during the different stages of the biofouling runs. In addition, where indicated, a continuous measurement of the permeate conductivity was carried out in a custom made glass flow cell (50 mL) designed for an Accumet conductivity probe (four-cell type with a cell constant of 1.0 cm^{-1}). Dissolved organic carbon analysis was conducted with a total organic carbon analyzer (Shimadzu TOC-V CSH). Prior to analysis, the 20 mL feed and permeate samples were filtered through a 0.22 μm syringe sterilized PVDF filter (Durapore).

2.5. Microscopy

2.5.1. Laser scanning confocal microscopy

At the end of each biofouling experiment with PA01 AH298, the membrane coupon was carefully removed and cut to pieces of around 5 mm × 5 mm for staining with either concanavalin A (ConA) conjugated to tetramethylrhodamine isothiocyanate (TRITC), or with propidium iodide (PI) for probing EPS or dead cells, respectively. Microscopic observation and image acquisition were performed using Zeiss-Axiovert 10, a laser scanning confocal microscope, equipped with Zeiss dry objective Plan-NeoFluar (10× magnification and numerical aperture of 0.3). The LSCM was equipped with detectors and filter sets for monitoring PI/TRITC stained cells and GFP (excitation wavelengths of 568 and 488 nm, respectively). LSCM images were generated using the BioRad confocal assistant software (Version 4.02). Gray scale images were analyzed, and the specific biovolume ($\mu m^3/\mu m^2$) in the biofouling layer was determined by COMSTAT, an image-processing software [50], written as a script in Matlab 5.1 (The MathWorks) and equipped with an image processing toolbox. Thresholding was fixed for all image stacks. At each time point, between 6 and 9 positions on the membrane were chosen and microscopically observed, acquired, and analyzed.

The ConA, conjugated to TRITC (Invitrogen Co.), was used as a probe to determine the presence of PA01 EPS [51,52]. Briefly, freezed (−20 °C) 100 μL aliquots of 1 mg/mL labeled ConA stock solution were prepared in 10 mM phosphate buffer (pH 7.5) and diluted to 100 μg/mL prior to use in 10 mM phosphate buffer (pH 7.5). Excess electrolyte solution was carefully drawn off from two pieces of a biofilm covered membrane by gently touching the edge of the specimens with an absorbing paper (Kimwipes) [51]. Then, 100 μL of ConA staining solution were added to cover the biofilm samples, which were then incubated in the dark at room temperature for 20 min. Unbound ConA was drawn off the specimens using a three-step wash of 10 mM phosphate buffer. The unbound ConA solution and the washing solutions were carefully removed by gently touching the edge of the specimen with an absorbing paper.

PI was used for probing dead cells in the biofouling layer. Excess electrolyte solution was carefully drawn off from a piece of a biofilm-covered membrane in the same manner used for ConA staining. Then, 100 μL of 3 μM PI solution (prepared in 10 mM phosphate buffer, pH 7.5) were added to cover the biofilm samples, which were then incubated in the dark at room temperature for 20 min. Excess PI solution was carefully drawn off with an absorbing paper. The excess PI nucleic acid stain that did not bind to the biofilm samples was then removed by rinsing three times with a 10 mM phosphate buffer at pH 7.5.

2.5.2. Environmental scanning electron microscopy (ESEM)

ESEM (FEI Company, Philips XL30) was used in a conventional high vacuum mode for imaging of the biofilm and dead cells. The biofilm or cells were fixed, dehydrated, and coated with a layer of carbon approximately 10–15 nm thick. The fixation method [53] involved the following steps: (1) excess electrolyte solution was carefully removed with a filter paper from the specimens (fouled membrane pieces of around 5 mm × 5 mm); (2) the fouled membrane specimens were incubated in 0.05 M sodium cacodylate buffer supplemented with 2% glutaraldehyde (Electron Microscopy Sciences, Fisher Scientific) for 1 h; (3) the specimens were incubated for 10 min and rinsed three times with 0.05 M sodium cacodylate buffer; (4) a second fixation step was performed by incubating the specimens in 0.05 M sodium cacodylate buffer supplemented with 1% osmium tetroxide for 1 h (Electron Microscopy Sciences, Fisher Scientific); (5) excess amounts of osmium tetroxide were removed according to the same procedure followed in step 3; (6) specimens were dehydrated during a 20 min incubation period in ethanol/water solutions with increasing ethanol concentrations (25, 50, 75, 95, and 100%); and (7) the specimens were washed once with hexamethyldisilazine (Electron Microscopy Sciences, Fisher Scientific) and dried overnight in a hood at room temperature.

3. Results and discussion

3.1. Influence of induced PA01 biofouling on membrane performance

In order to elucidate the mechanisms of RO membrane biofouling, a model bacterium, *P. aeruginosa* PA01, expressing a chromosomally unstable GFP, was used as a biofouling agent. *P. aeruginosa* is ubiquitous in soil and water, and has been isolated from biofilms of RO membranes originated from pre-treated secondary effluents [54]. Also, several other *pseudomonad* strains were found in secondary effluents and were used as model bacterial strains for biofouling studies [36,38,54–57]. In this study, biofouling was investigated under fixed conditions, namely dissolved organics, type of carbon and energy source, C/N ratio, oxygen concentration, pH, ionic composition, initial permeate flux, crossflow velocity, applied pressure, temperature, and membrane type. The effects of cell deposition and biofilm growth on membrane permeate flux and salt passage were characterized.

3.1.1. Permeate flux

Permeate flux decline was determined for four different experiments following inoculation of the RO unit with a late

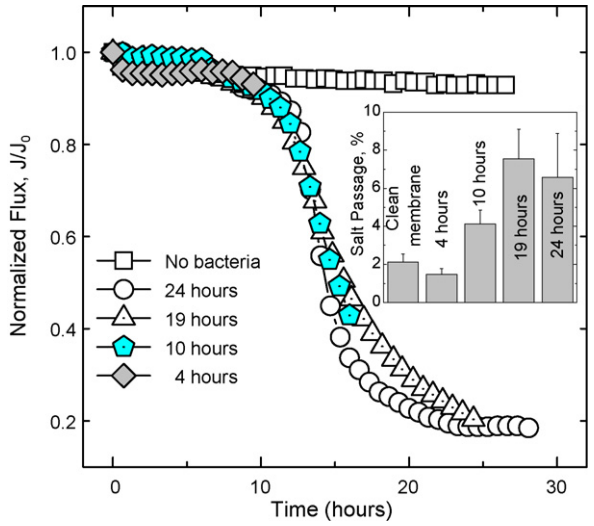

Fig. 1. Normalized flux decline upon induced biofouling with *P. aeruginosa* PA01 in four independent biofouling experiments terminated at different times. Also shown in the inset graph are the corresponding increases in salt passage at the end of the fouling runs. Experimental conditions were the following: initial permeate flux of 1.17 (±0.03) × 10^{-5} m/s (42.1 L/m^2 h or 24.8 gal/ft^2 day), crossflow velocity of 8.5 cm/s, initial cell concentration of 1.21 (±0.19) × 10^7 cells per mL, pH 7.4, and synthetic wastewater medium with a total ionic strength of 14.6 mM.

exponential culture of PA01, under enhanced biofouling conditions (Fig. 1). The four experiments were terminated at different times — 4, 10, 19, and 24 h — after inoculation of the bacteria. The initial cell concentration in the feed was adjusted to $1.21 \times 10^7 \pm 1.95 \times 10^6$ mL^{-1} in all the experiments. An identical permeate flux pattern was observed for an additional four experiments (data not shown), indicating good reproducibility of the results under the studied experimental conditions.

A minor flux decline was observed when bacteria were not inoculated in the RO unit (Fig. 1, open squares), probably due to the small amount of LB added to supplement growth factors and to enhance biofilm growth. This minor decrease in permeate flux indicates that there was no contamination in the RO unit that would contribute to growth of microorganisms at the expense of the medium added for enhanced biofouling. After a lag phase of 3–4 h, with only a slight decrease in permeate flux, a well characterized and reproducible drastic permeate flux decline is observed, where in less than 15 h, the permeate flux decreased to less than 20% of its initial value. Biofilm growth during this 15-h time period is the cause for the marked decrease in permeate flux as discussed later in the paper. The slight decrease in permeate flux immediately after inoculating the bacteria is probably due to a combination of both increased concentration polarization near the membrane surface caused by the addition of LB and ammonium chloride (30 min before inoculating the bacteria), and an immediate cell deposition on the membrane surface.

3.1.2. Salt passage

An increase in salt passage (measured by electric conductivity) is observed for the four different experiments and their replicates in Fig. 1 (inset graph). This increase of permeate conductivity was observed at the end of the three experiments which were terminated 10, 19, and 24 h after inoculating the bacteria. The increase in salt passage after a relatively short period of biofilm growth (between 4 and 18 h) is attributable to two factors. First, a significant increase in salt concentration in close proximity to the membrane surface upon growth of the biofouling layer can lead to enhanced salt transport across the membrane. As we discuss later, this substantial rise in salt concentration increases the trans-membrane osmotic pressure and subsequently decreases permeate flux (Fig. 1). Second, the significant decrease in permeate flux results in increased permeate salt concentration due to the so-called "dilution effect", thus resulting in decreased salt rejection. It should be emphasized that the synthetic wastewater solution is made up of a complex mixture with a large number of ionic species (Section 2.1), which precludes any mechanistic analysis and modeling of the rejection of the various ionic species under the complex biofouling conditions near the membrane surface.

3.2. Dynamics of biofilm growth

At the end of each of the biofouling experiments, the RO membrane coupon was carefully removed and stained with either propidium iodide or lectin concanavalin A conjugated to tetramethylrhodamine isothiocyanate to determine the changes in biovolumes of dead cells and EPS, respectively. ConA is a legume lectin, which binds to alginate α-D-mannuronate and α-D-guluronate residues, mainly through hydrogen bonding and van der Waals packing [58]. Recently, this protein has been extensively used as a probe to determine the presence and level of alginate expression in mucoid versus non-mucoid *P. aeruginosa* biofilms [51,52]. ConA has also been recently used for monitoring EPS in biofouling layers on RO [4] membranes fouled with *Sphingomonas* sp. and on MF membranes fouled with an uncharacterized microbial community in a submerged membrane bioreactor unit [59].

In this study, relatively short closed-loop, batch biofouling experiments were performed. By conducting different biofouling experiments, which were terminated at different times, we were able to monitor the dynamics of the biofouling layer deposition and growth. Fig. 2 presents representative LSCM image stacks, which were reconstructed as three-dimensional images using Imaris software (Bitplane, Switzerland). After only 4 h following the inoculation of the bacteria, microcolonies of PA01 expressing an unstable variant of GFP were observed (Fig. 2, 4 h after PA01 inoculation), and after 19 h, a cell layer with a thickness of approximately 30–40 μm was observed together with layers of EPS attached to the membrane surface (Fig. 2, 19 h after PA01 inoculation). Also, after 19 and 24 h, a dense and thick layer of dead cells was observed (Panel c), where more crevices and holes appeared after 24 h, probably due to detachment of cells and small aggregates from the biofilm. The different stages of biofilm formation observed on the RO membrane in these experiments show that the RO biofilm layer is changing rapidly over a relatively short period of time.

Biofilm growth dynamics for our experiments do not seem to follow previously reported biofilm developmental stages, where attachment, followed by growth of micro-colonies, biofilm mat-

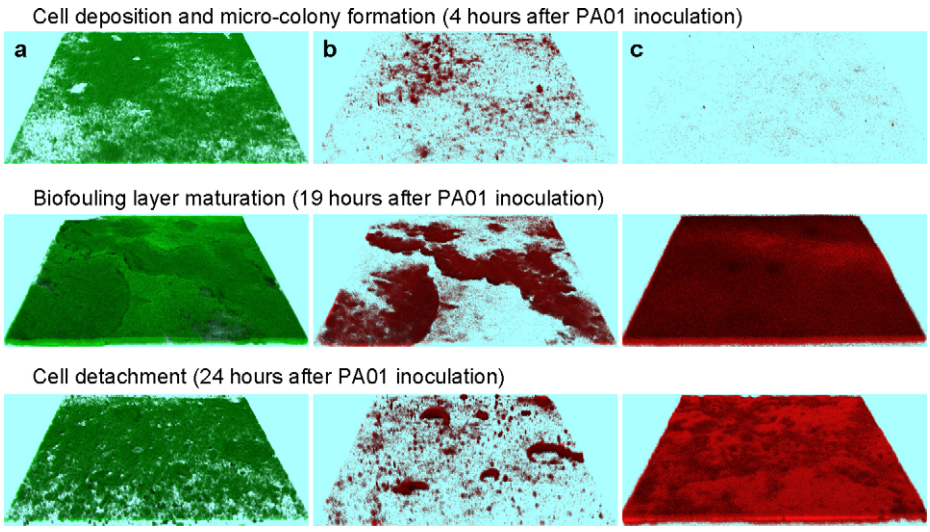

Fig. 2. A three-dimensional reconstruction using Imaris software (Bitplane, Zurich, Switzerland) of LSCM images taken from different biofouling runs (terminated at different times) from planar images acquired at depth intervals of 1 μm (the field of view for each figure is a perspective of 750 μm × 750 μm). Panels (a) and (b) are GFP and red fluorescent emissions, respectively, from the same specimen stained with concanavalin A conjugated to TRITC. Panel (c) shows dead cell specimens stained with propidium iodide. (For colour images, the reader is referred to the web version of the article.)

uration, and detachment are observed over a period of 4–6 days [60,61]. There are several possible reasons for the rapid biofilm dynamics observed here. First, initial cell deposition on the membrane surface is markedly enhanced, compared to other impermeable surfaces, because of the convective permeate flux. Second, depletion of nutrients occurs after 20–24 h, since the biofilm growth in our study is in batch mode, and degradation of at least 90% of the soluble total organic carbon (TOC) in the feed tank was observed 20 h after inoculating the bacteria (Fig. 3). Last, in previous reports [60,61], rich growth media were used, while a relatively defined minimal medium was applied in this study.

Quantitative analysis of the LSCM image stacks was conducted with COMSTAT [50], a three dimensional biofilm program. The specific biovolumes ($\mu m^3/\mu m^2$) of the different biofilm components, including viable cells (expressing an unstable GFP), dead cells (stained with propidium iodide), and EPS (by probing alginate residues with the lectin ConA) were obtained (Fig. 4a). The highest viable cell and EPS biovolumes are observed after 19 and 10 h, respectively, while more dead cells are observed in the biofilm after 24 h, most likely due to detachment of live bacteria. In fact, after 24 h, an increase in the viable bacterial count is observed for the suspended cells in the

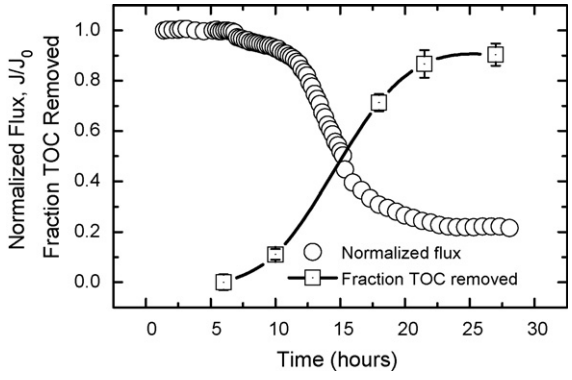

Fig. 3. Flux decline and TOC removal during biofouling of the RO membrane with *P. aeruginosa* PA01. Initial flux and TOC concentration were 1.23×10^{-5} m/s (44.3 L/m^2 h or 26.1 gal/ft^2 day) and 76.7 ± 2.4 mg/L, respectively. Other conditions are as those in Fig. 1.

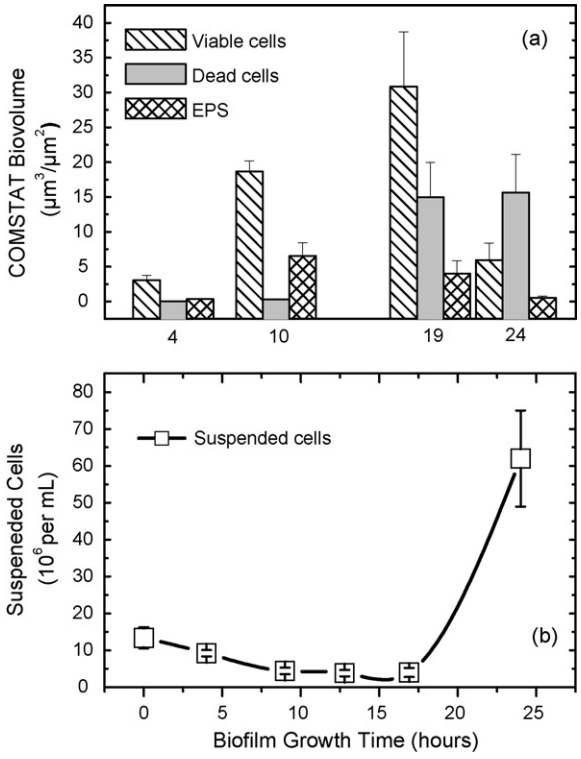

Fig. 4. (a) Specific biovolume of the biofouling layer components observed by LSCM and analyzed with COMSTAT for four independent experiments (described in Fig. 1) terminated at different times. (b) Viable cell count of *P. aeruginosa* PA01 in the suspended culture of the RO feed reservoir unit. The biofouling layer components are distinguished as follows: viable cells by GFP, dead cells by PI staining, and EPS by ConA staining.

feed reservoir (Fig. 4b), probably due to both cell detachment from the biofilm and growth of the suspended cells.

3.3. Membrane biofouling mechanisms

Biofilm growth on the RO membrane surface consisting of our model bacterial strain has been shown to induce permeate flux decline and increase salt passage. In the following discussion, the contribution of each of the biofilm components — bacterial cells and EPS — to the decrease in membrane performance will be assessed and the mechanisms involved will be delineated.

The contribution of bacterial cells (i.e., without the contribution of EPS) to flux decline was distinguished by the deposition of dead bacterial cells, pre-fixed with formaldehyde, on the membrane. Cells were added to the RO unit at a relatively high initial cell concentration (10^9 cells/mL, turbidity of 30.2 ± 0.8 NTU), in two replicates of fouling experiments conducted with the same synthetic wastewater used in the previous runs.

A sharp increase in salt passage is observed for the two separate experiments with dead cells (Fig. 5b), just *before* the onset of the decrease in permeate flux (Fig. 5a). This increase in salt passage indicates that salt concentration near the membrane surface is increased because back diffusion of salt is hindered by the deposited bacterial cells. The increase in salt concentration and consequently the osmotic pressure near the membrane surface is also the cause for the permeate flux decline in the experiments with dead cells. A similar observation has been recently reported for RO membranes in the presence of colloidal fouling [42,62]. The drastic flux decline caused by the deposited bacterial cells on the membrane (open circles and open diamonds) is lower than that caused by biofilm growth (open triangles), despite the very high cell concentration added to the unit. Therefore, the additional decrease in permeate flux in the presence of biofilm should be attributed to the EPS, as will be discussed later in this paper.

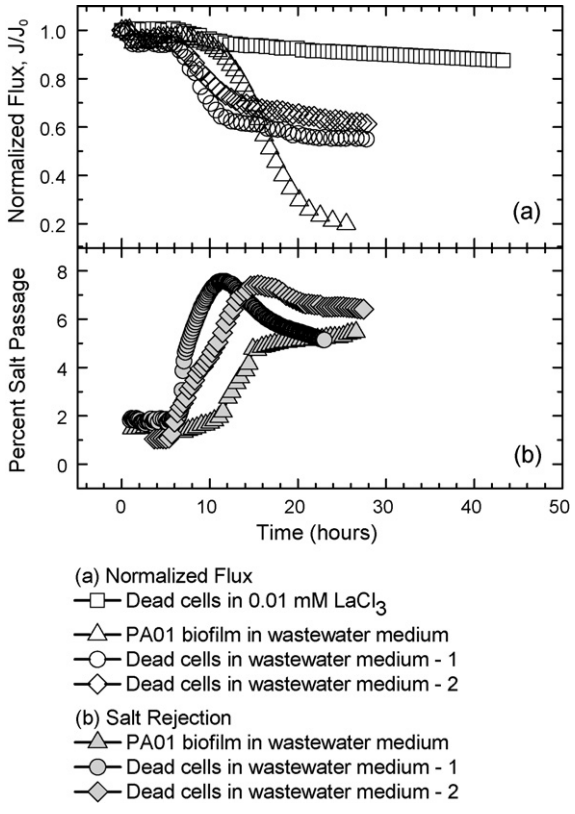

Fig. 5. Normalized flux decline (a) and salt passage (b) upon deposition of formaldehyde fixed PA01 dead cells (initial concentration of 10^9 cells/mL) and PA01 biofilm growth (initial concentration of 10^7 cells/mL) on the RO membrane in a synthetic wastewater medium (ionic strength of 14.6 mM and pH 7.4). Flux decline is also shown for *P. aeruginosa* PA01 dead cells (initial concentration of 10^9 cells/mL) in DI water supplemented with 0.01 mM $LaCl_3$ at pH 5.8.

In this proposed mechanism for biofouling, which until now has been demonstrated only for colloidal/particulate fouling [42,62], bacterial cells in the EPS matrix enhance concentration polarization near the membrane surface, which results in "biofilm-enhanced osmotic pressure". The enhanced salt buildup within the deposited cell layer and the associated increase in osmotic pressure at the membrane surface result in reduced permeate flux (Figs. 1 and 5). Permeate flux is shown to stabilize after 12 h of dead cell deposition using the synthetic wastewater electrolyte solution (Fig. 5a), while salt passage is decreasing and starts stabilizing at a much later time (Fig. 5b).

To verify the main mechanism by which bacterial cells decrease permeate flux, the increase in the hydraulic resistance by the deposited cell cake layer was evaluated. In contrast to the rapid permeate flux decline observed when the wastewater electrolyte solution was used, a relatively minor decrease in water flux was observed when dead cells were destabilized and deposited on the membrane with 0.01 mM $LaCl_3$ (Fig. 5a, open squares). The trivalent cation, La^{+3}, effectively reduces the electrostatic repulsion between the dead cells and between the dead cells and the membrane surface, thus resulting in the formation of a deposited cell cake layer. The low ionic strength of the added $LaCl_3$ (<0.1 mM) does not result in elevated osmotic pressure within the cake layer or the associated flux decline [42]. We note that the differences in feed turbidities between the time when cells were added and the end of the experiment were 2.8 ± 1.1 NTU and 2.4 ± 0.6 NTU for the dead cell fouling experiments with electrolyte solution and with 0.01 mM $LaCl_3$ solution, respectively. This observation indicates that the amounts of cells in the cake layers formed under these two solution conditions are comparable.

SEM images of the fouling layers formed from dead cells were taken at the end of the experiments with electrolyte solution and with $LaCl_3$ solution (Fig. 6a and b). While these images cannot be used as direct evidence to explain the occurrence of enhanced osmotic pressure within the deposited cell layer, they do suggest that the cells, after treatment with formaldehyde, were uniform without EPS components. It also appears that the porosities of the cake layers with electrolyte solution and with $LaCl_3$ solution are comparable. The negligible flux decline that occurs when ionic strength is minimized (i.e., with 0.01 mM $LaCl_3$), in combination with these SEM images, implies that the hydraulic resistance induced by the bacterial cake layer is small (relative to the membrane resistance), and therefore is a minor cause of flux decline. Hence, deposited bacterial cells induce permeate flux decline mainly due to hindered back diffusion of salt from the membrane surface, namely by "biofilm-enhanced osmotic pressure".

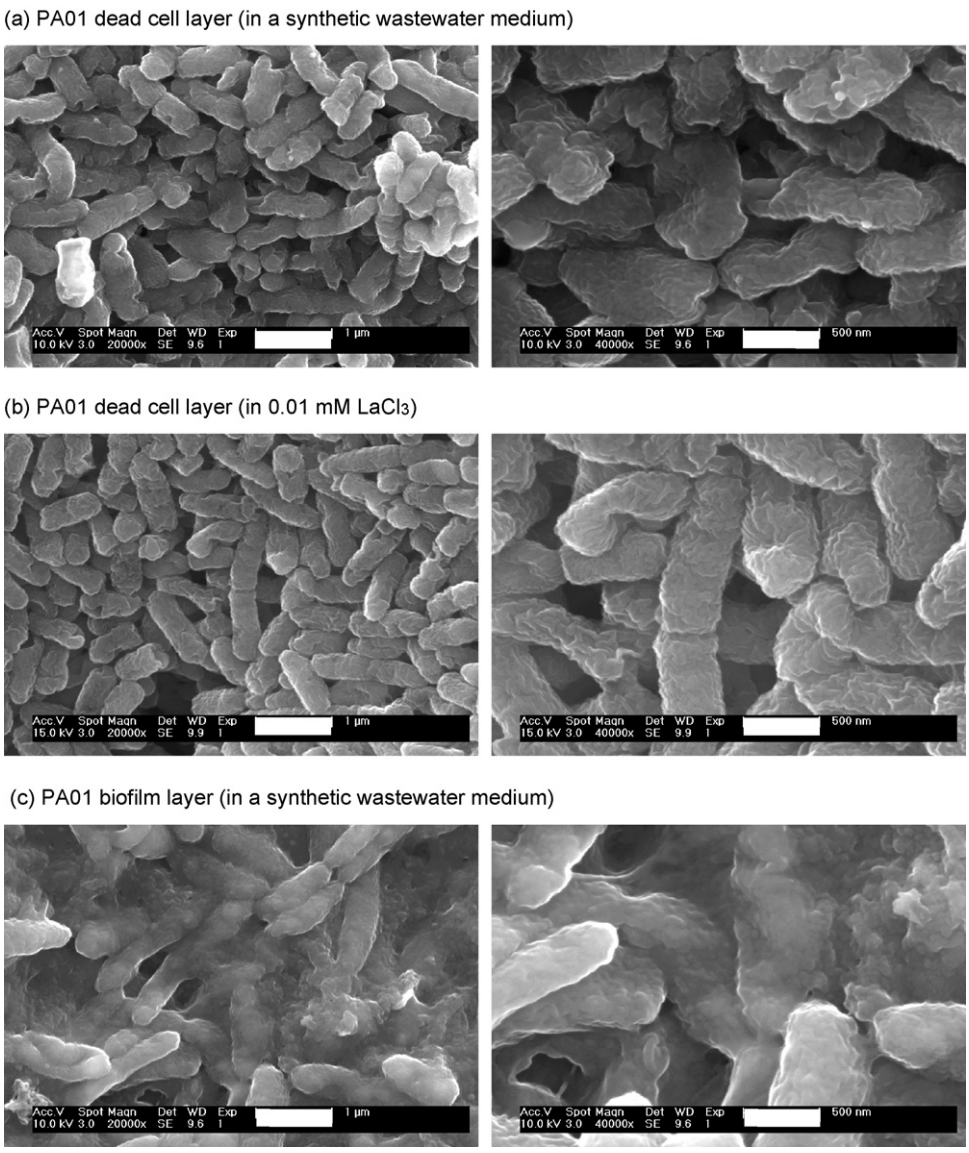

Fig. 6. SEM images of various *P. aeruginosa* PA01 biofouling layers. (a) Dead cells fixed in formaldehyde and deposited on the RO membrane in a synthetic wastewater medium after 23 h of deposition. (b) Dead cells fixed in formaldehyde and deposited on the RO membrane in DI water supplemented with 0.01 mM $LaCl_3$ after 38 h of deposition. (c) Live cells with their EPS (biofilm) grown for 19 h on the RO membrane in a synthetic wastewater medium. Scale bars (wide white line) on the left and right panels are 1 and 0.5 μm, respectively.

In order to better understand the relative contribution of EPS to the decrease in permeate flux and salt rejection, an evaluation of fouling caused by dead cells and by biofilm growth on the membrane is presented. The contribution of EPS to salt rejection is characterized by comparing the salt rejection for the biofouling experiments with the biofilm and with the dead cell cake layer (Fig. 5b). The comparable increase in salt passage induced by the dead cell cake layer and by the biofilm indicates that the addition of EPS to the fouling layer is likely not the main cause for the increase in salt passage. The results also suggest that EPS has no significant effect on the trans-membrane osmotic pressure. The additional flux decline that occurs when the biofilm fouls the membrane is likely attributed to the hydraulic resistance of the produced EPS. The opaque EPS matrix surrounding the cells (Fig. 6c) can provide hydraulic resistance to permeate flow, somewhat similar to observations of fouling of RO membranes by polysaccharides, such as alginate [48]. In contrast to the biofilm layer, the cake layer formed by dead cells is much more porous (Fig. 6b) and, as discussed earlier, provides negligible hydraulic resistance to permeate flow when compared to the RO membrane resistance.

Kim et al. [63] modeled the hindered diffusion of solutes within RO biofilms. In that paper, it has been suggested that large amount of EPS will reduce the void fraction between the cells and limit water permeation via the increase in hydraulic resistance. It is possible that EPS induces permeate flux decline by increasing biofilm hydraulic resistance to a larger extent than the contribution to hindered back diffusion from the membrane surface. In this case, convective mass transfer of salts from the bulk liquid may also be limited, such that the hindered back diffusion will be less pronounced.

4. Concluding remarks

The biofouling mechanisms of RO membranes and the impact of biofouling on membrane performance were investigated with a model bacterial strain (*P. aeruginosa*) under accelerated biofouling conditions. The deposition and growth of the biofouling layer followed the well known biofilm formation stages for *P. aeruginosa*, starting with formation of microcolonies, followed by maturation of the biofilm layer, and ending with detachment of bacterial cells. Biofouling of the RO membrane resulted in a sharp decline in permeate water flux and a concomitant drop in salt rejection. The decline in membrane performance was attributed to the increase in both the hydraulic resistance and the trans-membrane osmotic pressure of the fouled membrane. The increase in the trans-membrane osmotic pressure was attributed to the deposited bacterial cells, which enhanced the concentration polarization of salt near the membrane surface. An additional permeate flux decline was observed for the biofilm layer compared to the decrease in permeate flux upon fouling with dead cells alone. This additional flux decline is mainly attributed to the increase in hydraulic resistance by the EPS surrounding the bacterial cells.

Acknowledgments

This research was made possible by the WaterCAMPWS, a Science and Technology Center of Advanced Materials for the Purification of Water with Systems under the National Science Foundation agreement number CTS-0120978, and by a postdoctoral fellowship supplied by the United States-Israel Binational Agricultural Research and Development (BARD) fund. We also thank S. Molin from the Technical University of Denmark for providing us with *Pseudomonas aeruginosa* PA01 AH298 and Joseph S. Wolenski from the Molecular, Cellular, and Developmental Biology Department at Yale University for his help with the LSCM.

References

[1] S. Belfer, J. Gilron, N. Daltrophe, Y. Oren, Comparative study of biofouling of NF modified membrane at SHAFDAN, Desalination 184 (2005) 13–21.
[2] K.L. Chen, L. Song, S.L. Ong, W.J. Ng, The development of membrane fouling in full-scale RO processes, J. Membr. Sci. 232 (2004) 63–72.
[3] C. Jarusutthirak, G. Amy, Role of soluble microbial products (SMP) in membrane fouling and flux decline, Environ. Sci. Technol. 40 (2006) 969–974.
[4] C.M. Pang, P. Hong, H. Guo, W.-T. Liu, Biofilm formation characteristics of bacterial isolates retrieved from a reverse osmosis membrane, Environ. Sci. Technol. 39 (2005) 7541–7550.
[5] P. Xu, J.E. Drewes, T.-U. Kim, C. Bellona, G. Amy, Effect of membrane fouling on transport of organic contaminants in NF/RO membrane applications, J. Membr. Sci. 279 (2006) 165–175.
[6] R.M. Donlan, Biofilms: microbial life on surfaces, Emerging Infect. Dis. 8 (2002) 881–890.
[7] W.J. Costerton, Z. Lewandowski, D.E. Caldwell, D.R. Korber, H.M. Lappin-Scott, Microbial biofilms, Annu. Rev. Microbiol. 49 (1995) 711–745.
[8] R.P. Schneider, L.M. Ferreira, P. Binder, E.M. Bejarano, K.P. Goes, E. Slongo, C.R. Machado, G.M.Z. Rosa, Dynamics of organic carbon and of bacterial populations in a conventional pretreatment train of a reverse osmosis unit experiencing severe biofouling, J. Membr. Sci. 266 (2005) 18–29.
[9] H.-C. Flemming, G. Schaule, T. Griebe, J. Schmitt, A. Tamachkiarowa, Biofouling—the Achilles heel of membrane processes, Desalination 113 (1997) 215–225.
[10] J.A. Redman, S.L. Walker, M. Elimelech, Bacterial adhesion and transport in porous media: role of the secondary energy minimum, Environ. Sci. Technol. 38 (2004) 1777–1785.
[11] R. Bos, H.C. van der Mei, H.J. Busscher, Physico-chemistry of initial microbial adhesive interactions—its mechanisms and methods for study, FEMS Microbiol. Rev. 23 (1999) 179–229.
[12] S.L. Walker, J.A. Redman, M. Elimelech, Role of cell surface lipopolysaccharides in *Escherichia coli* K12 adhesion and transport, Langmuir 20 (2004).
[13] S.-T. Kang, A. Subramani, E.M.V. Hoek, M.A. Deshusses, M.R. Matsumoto, Direct observation of biofouling in cross-flow microfiltration: mechanisms of deposition and release, J. Membr. Sci. 244 (2004) 151–165.
[14] E. Bullitt, L. Makowski, Structural polymorphism of bacterial adhesion pili, Nature 373 (1995) 164–167.
[15] R.P. Schneider, K.C. Marshall, Retention of the Gram negative marine bacterium SW8 on surfaces—effects of microbial physiology, substratum nature and conditioning films, Colloids Surf. B: Biointerfaces 2 (1994) 387–396.
[16] J.T. Walker, P.D. Marsh, A review of biofilms and their role in microbial contamination of dental unit water systems (DUWS), Int. Biodeterior. Biodegrad. 54 (2004) 87–98.
[17] A.-C. Olofsson, M. Hermansson, H. Elwing, *N*-Acetyl-L-cysteine affects growth, extracellular polysaccharide production, and bacterial biofilm formation on solid surfaces, Appl. Environ. Microbiol. 69 (2003) 4814–4822.
[18] G.A. O'Toole, R. Kolter, Flagellar and twitching motility are necessary for *Pseudomonas aeruginosa* biofilm development, Mol. Microbiol. 30 (1998) 295–304.
[19] L.A. Pratt, R. Kolter, Genetic analysis of *Escherichia coli* biofilm formation: roles of flagella, motility, chemotaxis and type I pili, Mol. Microbiol. 30 (1998) 285–293.
[20] M. Rivera, E.J. McGroarty, Analysis of a common-antigen lipopolysaccharide from *Pseudomonas aeruginosa*, J. Bacteriol. 171 (1989) 2244–2248.
[21] M. Rivera, L.E. Bryan, R.E. Hancock, E.J. McGroarty, Heterogeneity of lipopolysaccharides from *Pseudomonas aeruginosa*: analysis of lipopolysaccharide chain length, J. Bacteriol. 170 (1988) 512–521.
[22] S. Makin, T. Beveridge, The influence of A-band and B-band lipopolysaccharide on the surface characteristics and adhesion of *Pseudomonas aeruginosa* to surfaces, Microbiology 142 (1996) 299–307.
[23] D.G. Davies, A.M. Chakrabarty, G.G. Geesey, Exopolysaccharide production in biofilms: substratum activation of alginate gene expression by *Pseudomonas aeruginosa*, Appl. Environ. Microbiol. 59 (1993) 1181–1186.
[24] D.M. Ramsey, D.J. Wozniak, Understanding the control of *Pseudomonas aeruginosa* alginate synthesis and the prospects for management of chronic infections in cystic fibrosis, Mol. Microbiol. 56 (2005) 309–322.
[25] G.A. O'Toole, H.B. Kaplan, R. Kolter, Biofilm formation as microbial development, Annu. Rev. Microbiol. 54 (2000) 49–79.
[26] C. Beloin, J.-M. Ghigo, Finding gene-expression patterns in bacterial biofilms, Trends Microbiol. 13 (2005) 16–19.
[27] K.D. Jackson, M. Starkey, S. Kremer, M.R. Parsek, D.J. Wozniak, Identification of *psl*, a locus encoding a potential exopolysaccharide that is essential for *Pseudomonas aeruginosa* PAO1 biofilm formation, J. Bacteriol. 186 (2004) 4466–4475.
[28] M. Matsukawa, E.P. Greenberg, Putative exopolysaccharide synthesis genes influence *Pseudomonas aeruginosa* biofilm development, J. Bacteriol. 186 (2004) 4449–4456.
[29] L. Friedman, R. Kolter, Two genetic loci produce distinct carbohydrate-rich structural components of the *Pseudomonas aeruginosa* biofilm matrix, J. Bacteriol. 186 (2004) 4457–4465.
[30] S. Comte, G. Guibaud, M. Baudu, Relations between extraction protocols for activated sludge extracellular polymeric substances (EPS) and EPS complexation properties: Part I. Comparison of the efficiency of eight EPS extraction methods, Enzyme Microb. Technol. 38 (2006) 237–245.

[31] H.-C. Flemming, Reverse osmosis membrane biofouling, Exp. Therm. Fluid Sci. 14 (1997) 382–391.
[32] H.-C. Flemming, Biofouling in water systems—cases, causes and countermeasures, Appl. Microbiol. Biotechnol. 59 (2002) 629–640.
[33] J.S. Vrouwenvelder, D. van der Kooij, Diagnosis, prediction and prevention of biofouling of NF and RO membranes, Desalination 139 (2001) 65–71.
[34] H.F. Ridgway, M.G. Rigby, D.G. Argo, Adhesion of a *Mycobacterium* sp. to cellulose diacetate membranes used in reverse osmosis, Appl. Environ. Microbiol. 47 (1984) 61–67.
[35] H.F. Ridgway, A. Kelly, C. Justice, B.H. Olson, Microbial fouling of reverse osmosis membranes used in advanced wastewater treatment technology: chemical, bacteriological, and ultrastructural analyses, Appl. Environ. Microbiol. 45 (1983) 1066–1084.
[36] H. Ivnitsky, I. Katz, D. Minz, E. Shimoni, Y. Chen, J. Tarchitzky, R. Semiat, C.G. Dosoretz, Characterization of membrane biofouling in nanofiltration processes of wastewater treatment, Desalination 185 (2005) 255–268.
[37] N. Park, B. Kwon, I.S. Kim, J. Cho, Biofouling potential of various NF membranes with respect to bacteria and their soluble microbial products (SMP): characterizations, flux decline, and transport parameters, J. Membr. Sci. 258 (2005) 43–54.
[38] H.F. Ridgway, H.-C. Flemming, in: J. Mallevialle, P.E. Odendaal, W.M.R. (Eds.), Membrane Biofouling in Water Treatment Membrane Processes, McGraw-Hill, 1996.
[39] D. Hasson, A. Drak, R. Semiat, Inception of $CaSO_4$ scaling on RO membranes at various water recovery levels, Desalination 139 (2001) 73–81.
[40] S. Hong, M. Elimelech, Chemical and physical aspects of natural organic matter (NOM) fouling of nanofiltration membranes, J. Membr. Sci. 132 (1997) 159–181.
[41] Y.A. Le Gouellec, M. Elimelech, Calcium sulfate (gypsum) scaling in nanofiltration of agricultural drainage water, J. Membr. Sci. 205 (2002) 279–291.
[42] E.M.V. Hoek, M. Elimelech, Cake-enhanced concentration polarization: a new fouling mechanism for salt-rejecting membranes, Environ. Sci. Technol. 37 (2003) 5581–5588.
[43] S. Lee, J. Cho, M. Elimelech, Combined influence of natural organic matter (NOM) and colloidal particles on nanofiltration membrane fouling, J. Membr. Sci. 262 (2005) 27–41.
[44] E. Werner, F. Roe, A. Bugnicourt, M.J. Franklin, A. Heydorn, S. Molin, B. Pitts, P.S. Stewart, Stratified growth in *Pseudomonas aeruginosa* biofilms, Appl. Environ. Microbiol. 70 (2004) 6188–6196.
[45] J. Sambrook, E.F. Fritsch, T. Maniatis, Molecular Cloning, A Laboratory Manual, second ed., Cold Spring Harbor Laboratory Press, Cold Spring Harbor, NY, 1989.
[46] G.S. Pettygrove, T. Asano, Irrigation with Reclaimed Municipal Wastewater: A Guidance Manual, California State Water Resources Control Board, Sacramento, CA, 1984, http://cee.engr.ucdavis.edu/Faculty/asano/IrrigationReuse1.pdf.
[47] E.M. Vrijenhoek, S. Hong, M. Elimelech, Influence of membrane surface properties on initial rate of colloidal fouling of reverse osmosis and nanofiltration membranes, J. Membr. Sci. 188 (2001) 115–128.
[48] W.S. Ang, S. Lee, M. Elimelech, Chemical and physical aspects of cleaning of organic-fouled reverse osmosis membranes, J. Membr. Sci. 272 (2006) 198–210.
[49] S. Lee, W.S. Ang, M. Elimelech, Fouling of reverse osmosis membranes by hydrophilic organic matter: implications for water reuse, Desalination 187 (2006) 313–321.
[50] A. Heydorn, A.T. Nielsen, M. Hentzer, C. Sternberg, M. Givskov, B.K. Ersboll, S. Molin, Quantification of biofilm structures by the novel computer program COMSTAT, Microbiology 146 (2000) 2395–2407.
[51] T.R. Neu, J.R. Lawrence, Lectin-binding analysis in biofilm systems, Methods Enzymol. 310 (1999) 145–150.
[52] M. Strathmann, J. Wingender, H.-C. Flemming, Application of fluorescently labelled lectins for the visualization and biochemical characterization of polysaccharides in biofilms of *Pseudomonas aeruginosa*, J. Microbiol. Methods 50 (2002) 237–248.
[53] E.N. Fox, R.S.J. Demaree, Quick bacterial microwave fixation technique for scanning electron microscopy, Microsc. Res. Techn. 46 (1999) 338–339.
[54] S.B. Sadr Ghayeni, P.J. Beatson, R.P. Schneider, A.G. Fane, Adhesion of waste water bacteria to reverse osmosis membranes, J. Membr. Sci. 138 (1998) 29–42.
[55] S.B. Sadr Ghayeni, P.J. Beatson, R.P. Schneider, A.G. Fane, Water reclamation from municipal wastewater using combined microfiltration-reverse osmosis (ME-RO): preliminary performance data and microbiological aspects of system operation, Desalination 116 (1998) 65–80.
[56] K.-J. Hwang, Y.-H. Yu, W.-M. Lu, Cross-flow microfiltration of submicron microbial suspension, J. Membr. Sci. 194 (2001) 229–243.
[57] G. Herath, K. Yamamoto, T. Urase, Mechanism of bacterial and viral transport through microfiltration membranes, Wat. Sci. Technol. 38 (1998) 489–496.
[58] W.I. Weis, Structural basis of lectin-carbohydrate recognition, Annu. Rev. Biochem. 65 (1996) 441–473.
[59] H.Y. Ng, T.W. Tan, S.L. Ong, Membrane fouling of submerged membrane bioreactors: impact of mean cell residence time and the contributing factors, Environ. Sci. Technol. 40 (2006) 2706–2713.
[60] M.M. Ramsey, M. Whiteley, *Pseudomonas aeruginosa* attachment and biofilm development in dynamic environments, Mol. Microbiol. 53 (2004) 1075–1087.
[61] B.R. Boles, M. Thoendel, P.K. Singh, Rhamnolipids mediate detachment of *Pseudomonas aeruginosa* from biofilms, Mol. Microbiol. 57 (2005) 1210–1223.
[62] E.M.V. Hoek, A.S. Kim, M. Elimelech, Influence of crossflow membrane filter geometry and shear rate on colloidal fouling in reverse osmosis and nanofiltration separations, Environ. Eng. Sci. 19 (2002) 357–372.
[63] A.S. Kim, H. Chen, R. Yuan, EPS biofouling in membrane filtration: an analytic modeling study, J. Colloid Interface Sci. 303 (2006) 243–249.